Shaped-Beam Circularly-Polarized Practical Antenna Array for Land Imaging SAR Systems

M. Abo El-Hassan [1], K. F. A. Hussein [1], A. E. Farahat [1], and K. H. Awadalla [2]

[1] Electronics Research Institute (ERI), Cairo, Egypt
mayaboelhassan@yahoo.com, Khalid_elgabaly@yahoo.com, asmaa@eri.sci.eg

[2] Faculty of Electronic Engineering, Menoufia University Egypt
kamal_awadalla@hotmail.com

Abstract — A planar array of $M \times N$ circularly polarized microstrip patch antennas is proposed for high resolution land-imaging applications using an airborne side-looking Synthetic Aperture Radar (SAR) systems. The microstrip patch is designed to produce either right-hand or left-hand circular polarization. The planar array is designed to produce a circularly polarized three-dimensional beam of cosecant-squared shape in the range direction and uniform shape in the azimuth direction. The mutual coupling between the adjacent patches in the proposed array is studied for the assessment of the final array design and is shown to have no bad effects on the resulting beam shape or the array performance. A computationally efficient Particle Swarm Optimization (PSO) algorithm is developed and applied to find the amplitude and phase distributions of the feeding voltages over the planar array elements required to produce the desired radiation patterns. This technique is achieved by developing a fast algorithm to extend the amplitudes and phases calculated for M-element and N-element linear arrays to be applied to the elements of a two-dimensional $M \times N$ planar array without the need to apply the PSO to calculate the amplitudes and phases for the entire elements of the planar array. A perfect three-dimensional pattern with the desired shapes in both azimuth and range directions is achieved. The input impedance, the axial ratio and the shapes of the radiation patterns produced by the proposed antenna array are investigated and shown to be satisfactory over the frequency band of $3.91 - 4.11$ GHz.

Index Terms — Axial ratio, beam shaping, cosecant squared, microstrip patch antenna, planar antenna arrays, PSO, synthetic aperture radar.

I. INTRODUCTION

The Synthetic Aperture Radar (SAR) system uses the time delay and Doppler information to generate a two-dimensional image with the desired range and azimuth resolutions, respectively [1]. This requires a SAR antenna with an aperture of high aspect ratio (the antenna aperture should be long in the azimuth direction and narrow in the range direction) and capable of achieving beam steering and beam shaping. A typical airborne or spaceborne side-looking SAR system uses an antenna with a beam that has a flat-top shape in the plane of the azimuth direction and a cosecant-squared shape in the plane of the range direction. This gives uniform illumination over the SAR beam footprint on the earth surface to get the incident power independent of the radar range for a constant height aircraft or spacecraft [2]. The planar arrays for both airborne and spaceborne SAR systems have many advantages including (i) its ability to achieve high aspect ratio of the antenna aperture that is long in the azimuth direction and narrow in the range direction and (ii) its ability to achieve the desired beam shapes in the two perpendicular azimuth and range directions.

Linearly polarized arrays are the most commonly used antenna type for SAR applications, especially for high-resolution land imaging. The currently used linearly polarized SAR systems are affected by Faraday's rotation during wave propagation from the satellite to the earth or random reflections from the atmospheric clutter [3]. Faraday's rotation is a result of the interaction of the propagating electromagnetic field and the earth's magnetic field. Some experimental SAR systems that use circular polarization are introduced in [4-6]. A SAR system which relies on circular polarization is proposed for a spaceborne platform [4]. An L-band circularly polarized SAR system that works at 1.275 GHz is introduced in [5] and compared to linearly polarized SAR system in a fully polarimetric experiment in an anechoic chamber. The comparison shows that circular polarization is less affected by the orientation angle of the target and could avoid the misalignment between the transmitter and receiver antenna during system operation. In [6] a complete fully polarimetric circularly polarized SAR system is developed for a microsatellite to observe land deformation on earth surface. However there is no beam shaping for the antenna array designed in [6]. The present

Submitted On: August 8, 2018
Accepted On: December 24, 2018

1054-4887 © ACES

work aims to produce accurately formed beam.

A circularly polarized antenna can be realized using arranged antennas of linear or circular polarized elements. In [7], a 2×2 planar antenna array of linearly polarized elements is introduced where unequal feed lines are used in order to produce two orthogonal electric fields with equal amplitudes and 90° phase difference. In [8], a feed network is used to split an input signal into four signals in phase quadrature and equal magnitudes and connected to four Vivaldi antennas sequentially rotated by 90º. Nevertheless, circular polarization can be produced using a single microstrip patch antenna with a single feed. Several methods have been proposed to provide circular polarization without the complexities inherent in dual-feed devices [9-10]. The design of a circularly polarized single-element single-feed microstrip patch antenna relies on the geometry of the antenna that enables the generation of two degenerate orthogonal modes to produce circularly polarized radiation. By introducing some asymmetry into the microstrip antenna geometry, the degeneracy of the two modes is removed. Examples of this technique are the square microstrip patch with a tilted slot, the corner-fed rectangular patch, the slightly elliptical patch, the pentagon-shaped patch, and the circular disc with perturbation element [11]. A compact single-feed circularly polarized microstrip antenna is proposed in [9] to achieve circular polarization over a wide beamwidth. In [10], a single-feed slotted circular microstrip patch antenna is introduced for operation in RFID applications. In the present work, a single-feed circularly polarized microstrip patch antenna is designed to operate as an array element for a land imaging side-looking SAR operating in the strip mapping mode at 4GHz. Arrays of such a microstrip patch are suitable for beam shaping and beam steering over a wide angular zone.

The methods of beam synthesis using antenna arrays depend on finding the complex excitation voltages of the array elements or the physical layout of the array that produces the radiation pattern close to the desired one. The most effective beam synthesis methods are the optimization techniques that depend on Evolutionary Algorithms (EAs). Several global optimization algorithms such as Differential Evolution (DE) [12], Genetic Algorithm (GA) [13], Simulated Annealing (SA) [14], and Ant Colony Optimization (ACO) have been used in antenna array pattern synthesis. The Particle Swarm Optimization (PSO) is one of the evolutionary optimization algorithms that are proposed in the present work to optimize the antenna pattern on the basis of the system requirements. The main objectives are to satisfy the required shape of the antenna main lobe and the minimum side lobe level within a specified mask pattern. The proposed PSO algorithm is simple, easy to implement and requires minimum mathematical processing.

In the following sections, the design of a single-feed Right-Hand Circularly Polarized (RHCP) as well as Left-Hand Circularly Polarized (LHCP) microstrip patch antenna are presented and the antenna characteristics including the input impedance, radiation pattern, axial ratio, and bandwidth are discussed. The mutual coupling, axial ratio and radiation patterns between two adjacent elements of such a patch arranged along x-axis and$y$-axis; for magnetic and electric coupling respectively; are investigated for different values of the separation distance. The PSO algorithm is applied to a 20-element linear array of microstrip patches to synthesize a cosecant-squared radiation pattern. It is also applied to a 10-element linear array to synthesize a fan-shaped beam. Finally, a proposed computationally efficient PSO is developed and applied to optimize the distribution of the excitation voltages of a planar array to achieve a cosecant-squared radiation pattern in the plane of the range direction and a flat-top radiation in the plane of the azimuth direction.

II. FOUR-SLOT TRUNCATED-CORNERS MICROSTRIP PATCH FOR CIRCULAR POLARIZATION

An asymmetric square microstrip patch, shown in Fig. 1, with four unequal circular sectors cut at the corners of the patch and four slots cut along the horizontal and vertical axes of symmetry is proposed to produce circular polarization. Such a microstip patch is intended to be used as an element for circularly polarized SAR antenna array. This microstrip patch is similar to that introduced in [15] with modifications to work at a frequency of 4 GHz. This microstrip patch has the advantages of low profile, lightweight, and ease of manufacturing using printed circuit techniques. The dimensional design parameters of the antenna are illustrated in Fig. 1. The substrate material is FR4 with dielectric constant $\varepsilon_r = 4.4$ and the loss tangent $\delta = 0.02$.The length of the square patch and the ground plane is denoted as L_P and G, respectively. As shown in Fig. 1, a coaxial feed is positioned at $x = 0, y = F$, where the origin is at the center of the microstrip patch. The radii of the four circular sector cuts are not equal and denoted as r_1, r_2, r_3, and r_4. Each of the four slots has length of L_s and width of W_s.The unequal truncated 90º circular sectors cut at the four corners of the square patch will produce two phase quad. This is required to produce circularly polarized rarature and spatially orthogonal modes with equal magnitudesdiated field.

A. Mechanism of producing circular polarization

The mechanism of producing circular polarization from such a microstrip patch can be attributed to electric field distribution in the four slots. The path of the surface current on the patch is truncated by each of the four slots causing the electric charges to be accumulated on the slot edges producing a strong horizontal electric field in the vertical slots, and a strong vertical electric field in the horizontal slots. The magnitudes of the vertical and

horizontal electric field components are nearly equal whereas the phase shift between them is about 90°, and thus, circularly polarized radiation is produced.

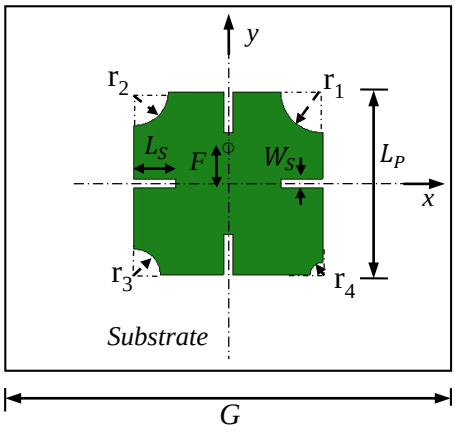

Fig. 1. Geometry of the proposed circularly polarized patch antenna.

B. Controlling the sense of polarization

By varying the sector radii of the truncated corner such that ($r1 > r2 > r3 > r4$) as shown in Fig. 2 (a), the patch antenna produces RHCP. By analogy, if the corner cuts are made such that ($r1 < r2 < r3 < r4$) as shown in Fig. 2 (b) the patch antenna produces LHCP.

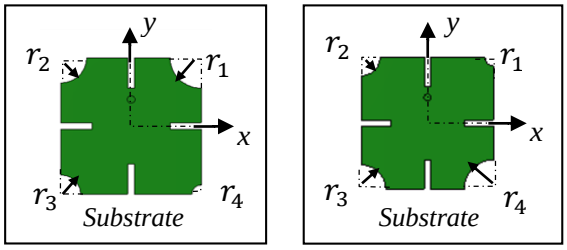

(a) Design for RHCP (b) Design for LHCP

Fig. 2. Controlling the sense of circular polarization produced by the patch antenna.

C. Mutual coupling between two adjacent patches

Consider two adjacent antennas fed by ports (1) and (2). According to the definition of the S_{21} parameter: it is the ratio of the voltage induced at port (2) to the voltage applied at port (1), which exactly expresses the mutual coupling between the two antennas. In a planar array arrangement the patch antenna will be repeated in two orthogonal directions (x- and y-directions). The effects of coupling between the elements in both directions are investigated. The distance between any two elements in the x or y-direction is denoted as d. For two elements arranged along the x-axis, the coupling coefficient is calculated for different separation distances. Also, the axial ratio and the circularly polarized radiation pattern are studied in the operating frequency range of the antenna for different separation distances between elements. The same parameters are calculated for two elements arranged along the y-axis. The two investigated configurations are shown in Fig. 3.

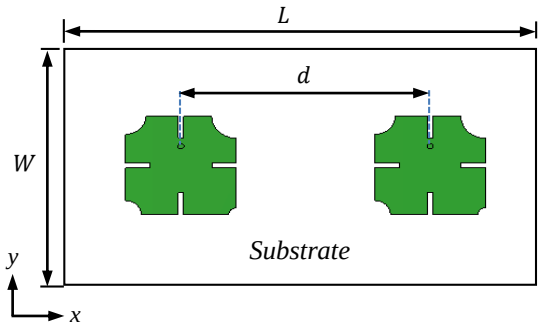

(a) Linear array arranged along x-axis

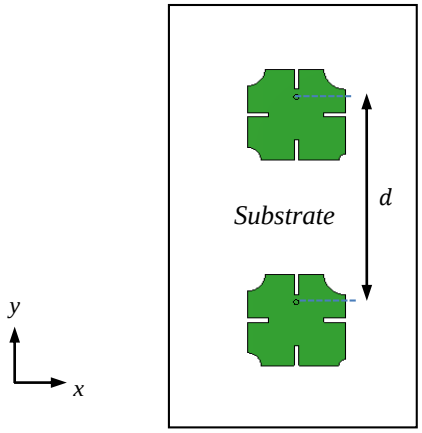

(b) Linear array arranged along y-axis

Fig. 3. Linear arrays of two patches,

III. PARTICLE SWARM OPTIMIZATION TECHNIQUE FOR LINEAR AND PLANAR ARRAYS

The Particle Swarm Optimization (PSO) is a popular optimization technique proposed for solving global numerical optimization problems. PSO technique is a robust stochastic evolutionary computation technique based on the movement and intelligence of swarms. It is simple to implement and quickly converges to good results. PSO has been used in the optimization of electromagnetic (EM) problems in the recent few decades [16]. In the present work, a computationally efficient PSO algorithm is developed to optimize the planar array radiation pattern to produce the beam shape required for land imaging SAR system. This beam is

cosecant-squared-shaped in the ground range direction and fan-shaped in azimuth direction. It aims to calculate the amplitude and phase of excitation for each element in the planar array. Such a radiation pattern can't be synthesized using one-dimensional array.

A. Conventional algorithm for PSO

The PSO algorithm is based on the analogy of movement of bird flocks or fish schools on one side, and the optimization on the other side. The PSO algorithm searches for the global minimum of the cost function, i.e., minimizes the cost function of an electromagnetic problem by simulating movement and interaction of particles (agents) in a swarm. The position of a particle corresponds to one possible solution of the EM problem, i.e., it corresponds to one point in the optimization space. The velocity and position update equations for the swarm particles are given in [17].

As the main goal of the PSO during its iterations is to reduce the cost function, the latter should be increased as the achieved radiation pattern further deviates from the ideal pattern. Thus, the cost function can be, simply, the absolute difference between the achieved and the desired (ideal) patterns of the electric field as follows:

$$F_C = \left|E(\theta) - \hat{E}(\theta)\right|. \tag{1}$$

In conclusion, the amplitudes and phases of excitation are determined by the PSO algorithm so as to satisfy the required beam shape and the remaining objectives of the antenna array design such as the axial ratio and the sidelobe level.

B. Development of computationally efficient PSO algorithm for planar arrays

Assuming that the array elements are arranged in N_x rows and N_y columns; the rows are perpendicular to the x-axis whereas the columns are perpendicular to the y-axis. The electric field radiated in the far zone can be expressed as [18]:

$$E(\theta,\phi) = \sum_{n_x=1}^{N_x}\sum_{n_y=1}^{N_y} A_{n_x,n_y} e^{j\varphi_{n_x,n_y}} \times e^{jk_o((n_x-1)D_x cos\phi + (n_y-1)D_y sin\phi)sin\theta}, \tag{2}$$

where, D_x is the separation between successive rows, D_y is the separation between successive columns and $A_{n_x,n_y}$and $\varphi_{n_x,n_y}$are the magnitude and phase of the excitation voltage, respectively, for the array element lying in the row number n_x and the column number n_y.

Thus, to get the beam produced by the planar array oriented in the direction (θ_o, ϕ_o), the phase of the excitation of each element in the planar array should be given as:

$$\varphi_{n_x,n_y} = -k_o\left[(n_x-1)D_x cos\phi_o + (n_y-1)D_y sin\phi_o\right] sin\theta_o. \tag{3}$$

On the other hand, the amplitudes of the excitation A_{n_x,n_y} are left to be determined by the PSO algorithm so as to satisfy the remaining objectives of the antenna array design

Applying the PSO algorithm on a planar array is much time-consuming. The amplitude of the excitation of each element of the planar array expressed as the product of two multiplicands; that is:

$$A_{n_x,n_y} = A_{x_{n_x}} A_{y_{n_y}}. \tag{4}$$

On the other hand, the phase of excitation of each element of the planar array expressed as the product of the sum of two angles; that is:

$$\varphi_{n_x,n_y} = \varphi_{x_{n_x}} + \varphi_{y_{n_y}}. \tag{5}$$

Equation (2) can be written as the product of two multiplicands:

$$E(\theta,\phi) = \sum_{n_x=1}^{N_x} A_{x_{n_x}} e^{j\varphi_{x_{n_x}}} e^{jk_o(n_x-1)D_x sin\theta\, cos\phi} \times \sum_{n_y=1}^{N_y} A_{y_{n_y}} e^{j\varphi_{y_{n_y}}} e^{jk_o(n_y-1)\,D_y sin\theta\, sin\phi}, \tag{6}$$

or simply,

$$E(\theta,\phi) = E^{(Lx)}(\theta,\phi) \times E^{(Ly)}(\theta,\phi), \tag{7}$$

where,

$$E^{(Lx)}(\theta,\phi) = \sum_{n_x=1}^{N_x} A_{x_{n_x}} e^{j\varphi_{x_{n_x}}} e^{jk_o(n_x-1)D_x sin\theta\, cos\phi}, \tag{8}$$

and,

$$E^{(Ly)}(\theta,\phi) = \sum_{n_y=1}^{N_y} A_{y_{n_y}} e^{j\varphi_{y_{n_y}}} e^{jk_o(n_y-1)\,D_y sin\theta\, sin\phi}. \tag{9}$$

It should be noticed that (8) gives an expression for the electric field radiated from a linear array of point sources arranged along the x-axis, whereas (9) gives an expression for the electric field radiated from a linear array of point sources arranged along the y-axis. In the special case of a beam which is symmetric about the direction of its maximum (θ_o, ϕ_o), the array elements are fed with progressive phase shifts in the x and y directions given, respectively, by the following expressions:

$$\Delta\varphi_x = -k_o D_x\, sin\theta_o\, cos\phi_o, \tag{10}$$

$$\Delta\varphi_y = -k_o D_y\, sin\theta_o\, sin\phi_o. \tag{11}$$

Consequently, the phases are given by:

$$\varphi_{x_{n_x}} = -k_o(n_x-1)\,D_x\, sin\theta_o\, cos\phi_o, \tag{12}$$

$$\varphi_{y_{n_y}} = -k_o\left(n_y-1\right)D_y\, sin\theta_o\, sin\phi_o. \tag{13}$$

In this case, the PSO algorithm can be run to optimize the shape of the radiation pattern (8) by iteratively setting the amplitudes $A_{x_{n_x}}$. In the same manner, the PSO algorithm can run to optimize the shape of the radiation pattern (9) by iteratively setting the amplitudes $A_{y_{n_y}}$.

The optimization process to obtain a symmetric beam shape from a planar array using the PSO algorithm that runs to optimize linear arrays can be described as follows.

1- Consider that planar array lies in the *x*-*y* plane and consider the required beam with its desired shape is oriented normal to the array plane (*z*-direction). This means to set $\varphi_{x_{n_x}} = 0$ and $\varphi_{y_{n_y}} = 0$ for all the array elements in both equation (8) and equation (9).
2- Give expression to describe the (ideal) beam shapes in *z*-*x* and *y*-*z* planes as $E_{opt}^{(Lx)}(\theta, 0)$ and $E_{opt}^{(Ly)}(\theta, \pi/2)$.
3- Apply PSO algorithm to optimize $E^{(Lx)}(\theta, \phi)$ given by equation (8) after setting $\varphi_{x_{n_x}} = 0$ and $\phi = 0$. This determines the optimum values of $A_{x_{n_x}}$.
4- Apply PSO algorithm to optimize $E^{(Ly)}(\theta, \phi)$ given by equation (9) after setting $\varphi_{y_{n_y}} = 0$ and $\phi = \pi/2$. This determines the optimum values of $A_{y_{n_y}}$.
5- Calculate A_{n_x,n_y} using equation (4).
6- Calculate φ_{n_x,n_y} using equation (3) to get the shaped beam oriented at (θ_o, ϕ_o).
7- Finally, calculate the total radiated electric field using the expression in equation (2).
8- Using this method, the approximate run time required for the PSO algorithm to optimize two-dimensional planar antenna array is only twice the time required to optimize the one-dimensional linear antenna array.

IV. RESULTS AND DISCUSSIONS

It may be worthwhile to mention that a circularly polarized patch antenna of the same type as that proposed in the present work, is introduced in [15] and is designed to operate for global navigation satellite systems in the frequency band (1.566–1.582GHz). In the present work, the design of the same type of patch antenna is modified to operate for land imaging SAR systems in the frequency band (3.91 to 4.11 GHz). The CST commercially available electromagnetic simulation package is used for assessment of the antenna performance. The optimal design parameters of the patch antenna to produce RHCP are $L_P = 16.4$ mm, $G = 44$ mm, $r_1 = 3.65$ mm, $r_2 = 3$ mm, $r_3 = 2.31$ mm, $r_4 = 1.1$ mm, $L_s = 3.6$ mm, $W_s = 0.8$ mm, $F = 3.2$ mm, $h = 1.5$ mm, $\varepsilon_r = 4.4$ mm, and $\delta = 0.02$. It should be noted that in the following presentation and discussions of the numerical results the patch antenna has the same design parameters listed above unless otherwise indicated.

A. The mechanism of producing circular polarization

A RHCP patch supports two orthogonal modes with equal magnitudes and 90˚ phase difference. This is realized by cutting the four unequal 90˚ circular sectors at the four corners of the microstrip patch. To demonstrate the mechanism of producing circular polarization, the surface current distributions at different phase angles of the wavelength at 4 GHz are shown in Fig. 4, namely at phases 0°, 45°, 90°, and 135° which are corresponding to the 0, 1/8, 1/4, and 3/8 of the periodic time of the microwave oscillation. At a phase of 0°, the current density on the patch surface is concentrated around the two vertical slots (along the *y*-axis), which generates *x*-directed electric field in the vertical slots. At phase of 90°, the surface currents are mainly concentrated around the horizontal slots (along the *x*-axis) producing *y*-directed electric field in the horizontal slots. At a phase of 45°, the charge concentration around the four slots is almost the same resulting in equal electric field magnitudes in both *x*- and *y*-directions, with a resultant electric field inclined 45° to the horizontal or vertical axis. Thus a circulating electric field is produced between phases 0° and 90°, i.e., the electric field vector generated in the near zone will change its direction from pure E_x component at phase 0°, to pure E_y component at phase 90°. This produces a circularly polarized electric field in the far zone rotating in the same direction.

B. Frequency band of operation of the circularly polarized patch antenna

The simulation results for the reflection coefficient of the proposed patch antenna considering a feed line of **50Ω** characteristic impedance against the frequency are shown in Fig. 5. The return loss is maintained below $-10\ dB$ in the frequency range **3.91GHz** to **4.11GHz** (**200MHz**). In the same figure, the axial ratio is plotted against the frequency where it is maintained below **3dB** through the frequency range **3.984 GHz to 4.027 GHz** (43 MHz). Thus the antenna bandwidth for acceptable performance can be considered (**3.984 − 4.027 GHz**).

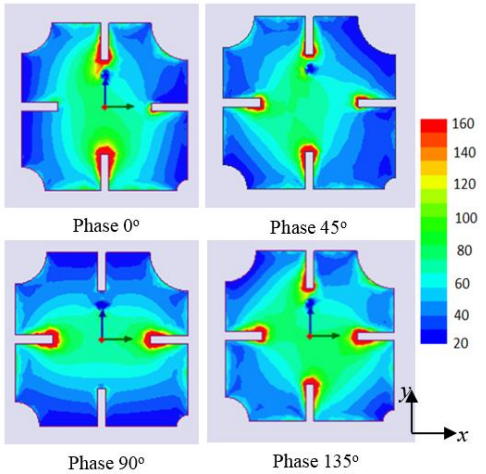

Fig. 4. Current distribution (A/m) on the surface of a microstrip patch at different phase angles.

A prototype of a single patch antenna is fabricated in the laboratory for experimental verification of the simulation results concerning the dependence of the return loss on the frequency. Top and bottom views of the fabricated antenna are presented in Fig. 6 (a), the vector network analyser of the Agilent Field Fox N9918A is used to measure $\boldsymbol{S_{11}}$ at the antenna port against the frequency. Figure 6 (b) shows the experimental setup with the fabricated prototype of the proposed antenna. A comparison between the experimental and simulation results of the return loss of the antenna shows good agreement as shown in Fig. 7.

C. Radiation patterns of circularly polarized fields

For experimental assessment of the RHCP radiation pattern, the dual circular polarized antenna model JXTXLB-OSJ-20180 is used as a reference antenna and the experimental setup is made as shown in Fig. 8.

A good agreement between the experimental and simulation results of the right-hand circularly polarized radiation patterns of the patch antenna is shown in Fig. 9. The radiation patterns are measured at 4 GHz in the two principal planes $x-z$ ($\phi = 0°$) and $y-z$ ($\phi = 90°$). It is clear in the figure that the radiation is dominated by right-hand circularly polarized electric field component.

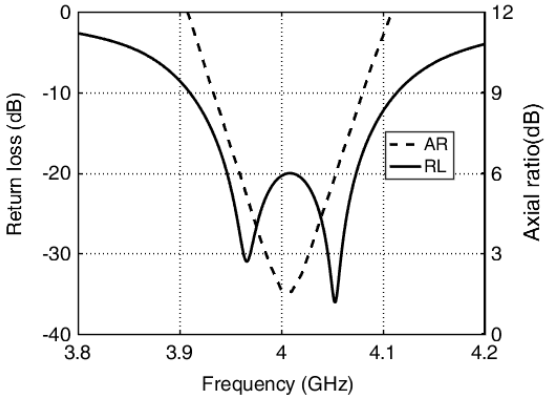

Fig. 5. Simulated return loss and axial ratio versus frequency for the circularly polarized patch antenna with the geometry presented in Fig. 1.

Top view Bottom view

(a) Top and bottom views of the fabricated prototype

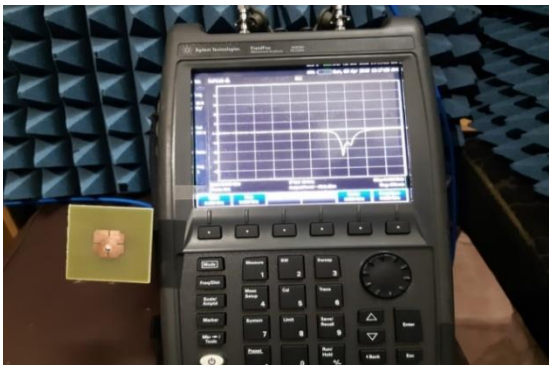

(b) Experimental setup for measuring S_{11}

Fig. 6. Experimental measurements of the circularly polarized patch antenna.

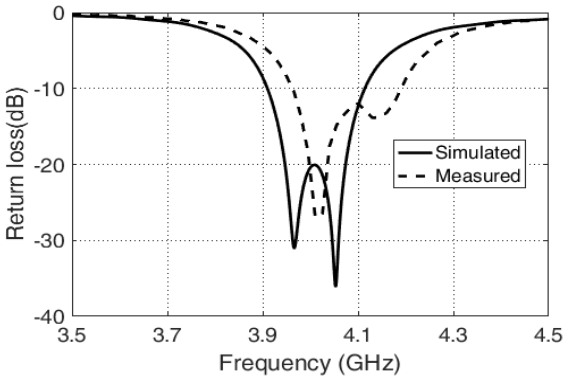

Fig. 7. Frequency dependence of the experimentally measured S_{11} for the fabricated antenna compared with the simulation results.

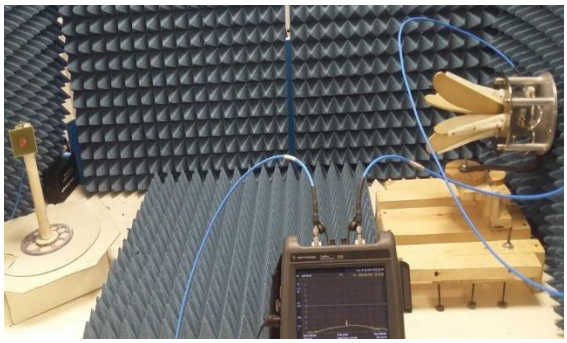

Fig. 8. Experimental setup for measurement of the antenna radiation patterns.

D. Beam width of circular polarization of a single patch antenna

The axial ratio, as a function of the angle θ, is shown in Fig. 10 for the two principle planes $\phi = 0°$ and $\phi = 90°$ at a frequency of 4 GHz. It is clear that the 3 dB axial ratio beam width is about 110° in the plane $\phi = 0°$ and about 180° in the plane $\phi = 90°$. This is considered

good radiation characteristics of a single-element to synthesize the beam shapes required for land imaging SAR applications using planar arrays of such an element.

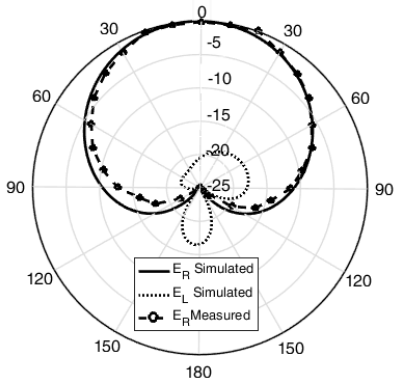

(a) Radiation patterns in the plane $\phi = 0°$

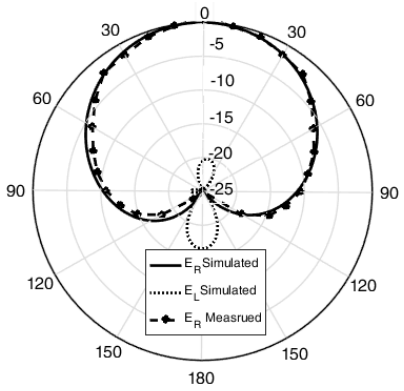

(b) Radiation patterns in the plane $\phi = 90°$

Fig. 9. Simulated and measured radiation patterns for RHCP and LHCP of the microstrip patch prototype presented in Fig. 1.

E. Coupling between two adjacent patch antennas

Mutual coupling between array elements is an important factor that may affect the performance of an antenna array, especially the coupling between adjacent elements. In printed antennas the mutual coupling mainly arises due to either the currents induced by the near field coupling from the other antennas or the surface waves on the substrate. By reducing the mutual coupling between array elements, the scan blindness effects will be reduced and the implementation of beam shaping will be much easier [18].

The coupling between two adjacent elements of the microstrip antenna is studied both computationally by simulation and experimentally using a vector network analyzer. Two elements of the proposed microstrip patch antenna are arranged in two configurations. In one of them the two elements are arranged along the x-axis and in the other configuration, the elements are arranged along the y-axis as shown in Fig. 3 (a) and Fig. 3 (b), respectively. The effect of the variation of the distance between the two elements on the coupling coefficient (S_{21}) over the frequency band $3.8 - 4.2$GHz can be explained in view of the plots of S_{11} and S_{21} presented in Fig. 11 for separation distances of 22 mm, 30 mm, and 37 mm for both arrays. It is clear from the figure that the coupling between the two elements decreases as the distance increases for both array configurations. For all the separation values, the magnitude of S_{11} and S_{21} presents weak coupling, which is a promising result for a subsequent beam shaping process using planar arrays.

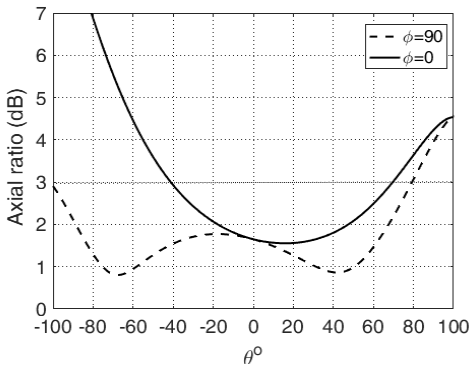

Fig. 10. Axial ratio in the elevation planes $\phi = 0°$ and $\phi = 90°$ for the patch antenna presented in Fig. 1 at 4 GHz.

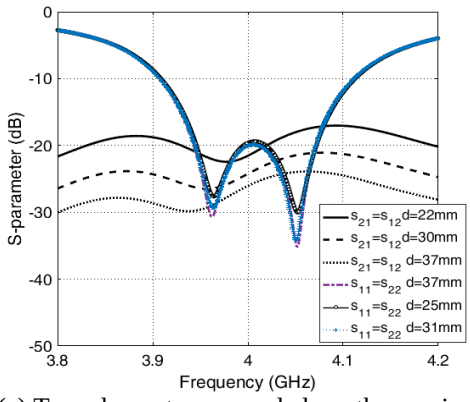

(a) Two elements arranged along the *x*-axis

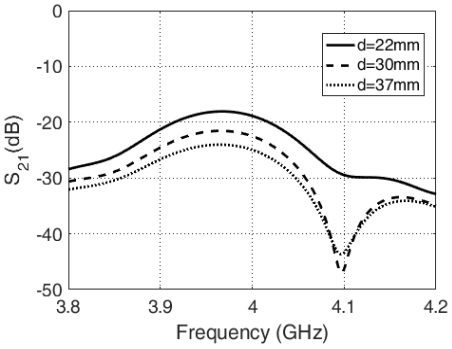

(b) Two elements arranged along the y-axis

Fig. 11. Mutual coupling between two adjacent patches for different values of the separation distance.

Two-element arrays of the circularly polarized patch antenna are laboratory fabricated to get two different configurations: one in which the elements are arranged along x-axis and the other in which the elements are arranged along y-axis. The separation between the two elements is 37 mm ($\lambda/2$) for both array configurations. Photographs for both fabricated arrays are presented in Fig. 12. The setup for measuring the radiation pattern is presented in the same figure.

The coupling coefficient between the two ports (S_{21}) is measured using a vector network analyser. Figure 13 presents comparisons between the simulation and measurement results for S_{21} for both antenna arrangements. The comparisons show good agreement.

Top view Bottom view

(a) Fabricated *x*-arranged array

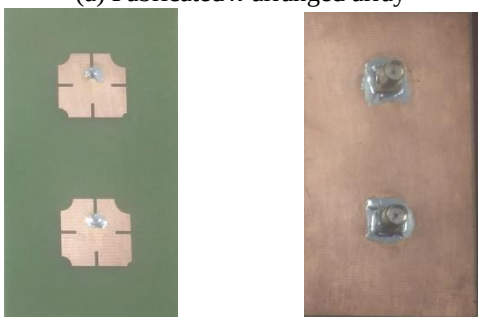

Top view Bottom view

(b) Fabricated *y*-arranged array

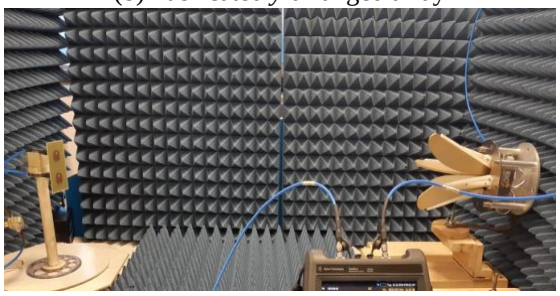

(c) Experimental setup for radiation pattern measurements

Fig. 12. Photographs for fabricated arrays of the circularly polarized antenna and the experimental setup for radiation pattern measurements.

It is also important to study the dependence of the 3dB axial ratio beam width of the two-element arrays on the separation between the elements. In Figs. 14 and 15, the axial ratio is plotted against θ at 4 GHz for separation distances of 22mm, 30 mm, and 37 mm in the planes $\phi = 0°$and $\phi = 90°$, respectively.

It is clear that the separation distance has a significant effect on the beam width over which the axial ratio is maintained below 3dB. The separation distance has a greater effect on the 3dB axial ratio beam width for the array arranged along the y-axis than that effect on the array arranged along the x-axis. For the y-arranged array the 3dB axial ratio beam width in the plane $\phi = 0°$ changes from 180° for a separation distance of 22mm to about 90° for a separation distance of 37mm. For the same array the 3dB axial ratio beam width in the plane $\phi = 90°$changes from 115° for a separation distance of 22 mm to about 60° for a separation distance of 37 mm. For the x-arranged array the 3dB axial ratio beam width in the plane $\phi = 0°$changes from 110° for a separation distance of 22mm to about 83° for a separation distance of 37mm. The 3dB axial ratio beam width of the x-arranged array in the plane $\phi = 90°$ seems to have insignificant dependence on the separation between the adjacent elements.

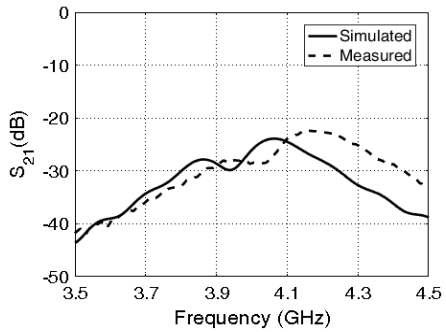

(a) Two-element array arranged along the *x*-axis

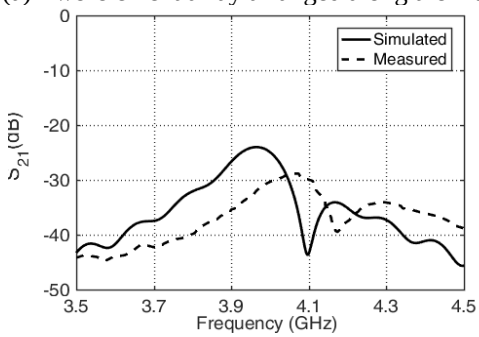

(b) Two-element array arranged along the *y*-axis

Fig. 13. Comparison between the experimental and simulation results for the frequency behavior of the coupling coefficient S_{21} for both array arrangements at separating distance of $\lambda/2$ between the array elements.

Comparisons between the experimental and simulation results for the patterns of the circularly polarized fields radiated by both the *x*-arranged and *y*-arranged array configurations are presented in Fig. 16 and Fig. 17, respectively. The radiation patterns are plotted in the plane of the array arrangement (i.e., in the plane $\phi = 0°$ for x-arranged array and in the plane

$\phi = 90°$ for the y-arranged array). The comparisons show good agreement between the computational and experimental results.

V. BEAM SHAPING USING CIRCULARLY POLARIZED PLANAR ARRAYS OF PATCH ANTENNAS

In the present section, the PSO algorithm is applied to set the proper amplitude and phase distributions of the feeding voltages over linear arrays of the proposed asymmetric circularly polarized patch antennas. Each element in the array has a separate coaxial feeder but the array is placed over a common substrate and ground plane.

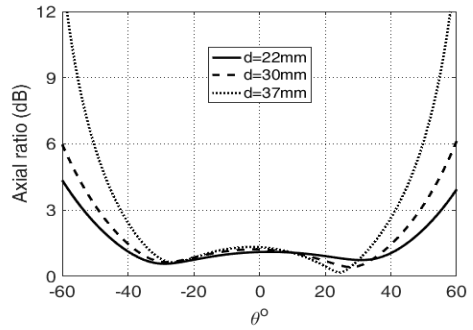

(a) $\phi = 0°$

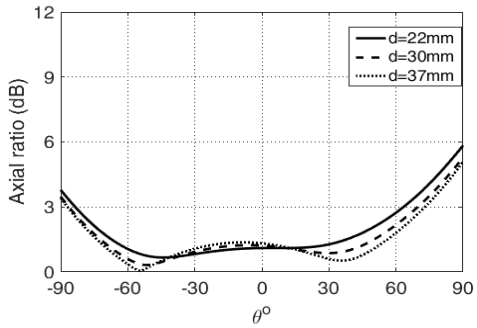

(b) $\phi = 90°$

Fig. 14. Axial ratio versus θ for two-element array arranged along x-axis for different values of the separation distance at 4 GHz.

The side-looking imaging SAR radiation pattern has cosecant-squared shape in the range direction and fan shape in the cross-range (azimuth) direction. The cosecant-squared radiation pattern provides a uniform earth illumination where the received power is independent of the range distance between the SAR and the imaged land. It is a means of achieving more uniform signal strength at the input of the receiver of the SAR system. In the azimuth direction the radiated beam should have a flat-top beam to ensure uniform distribution of the power density over the illuminated area in the azimuth direction.

The three-dimensional radiation pattern required for land imaging side looking SAR system has cosecant-squared shape in the range direction and uniform (flat-top) shape in the azimuth direction. This pattern cannot be achieved unless a planar array is used to synthesize the required beam shapes in the two orthogonal planes. In a similar way to that applied for beam shaping using linear arrays, the PSO algorithm is, first, applied to optimize the beam produced by a planar array of 20×10 point-source elements in the x-direction and y-direction respectively, through the control of the amplitudes and phases of excitation voltages to obtain cosecant-squared beam shape in the range direction ($\phi = 0°$ plane) within the angular zone $-15° < \theta < 15°$and fan-shaped beam in the azimuth direction ($\phi = 90°$ plane) within the angular zone $-20° < \theta < 20°$.

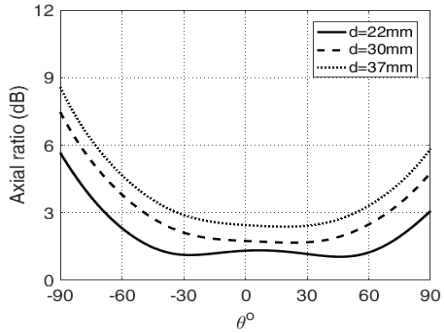

(a) $\phi = 0°$

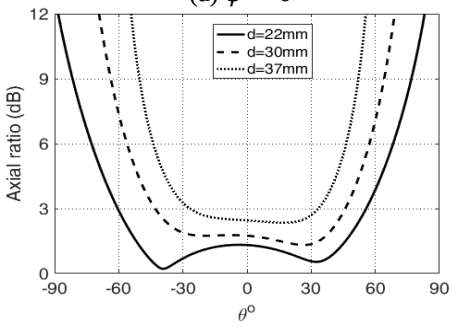

(b) $\phi = 90°$

Fig. 15. Axial ratio versus θ for two-element array arranged along y-axis for different values of the separation distance at 4 GHz.

The excitation coefficients are calculated as described in Section III.B for optimizing the radiation pattern of a planar array. The obtained excitation voltages are then applied to an array of 20×10 elements of the circularly polarized microstrip patches through electromagnetic simulation using CST© commercial package at 4.0 GHz. The array elements are placed over a comman ground plane and fed through 20×10 symmetrical 50Ω SMA coaxial feed points. The separation distance between the contiguous patches is 0.4λ in both x- and y-directions and the total array antenna size is 614mm×314 mm. The resulting RHCP radiation patterns are shown in Fig. 18 in both $\phi = 0°$and $\phi = 90°$ planes and compared to

the ideal (desired) beam shape. The axial ratio is plotted in the same figure in both planes, where it is shown to be maintained below 3dB within the angular zone of interest. The average error between the desired radiation pattern and the actually achieved radiation pattern is about 6.6 %.

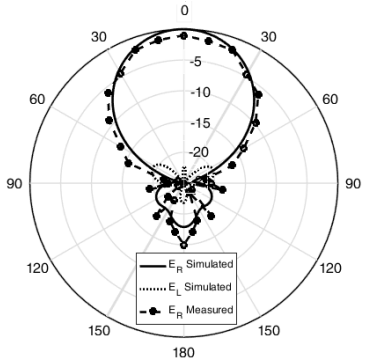

(a) $\phi = 0°$

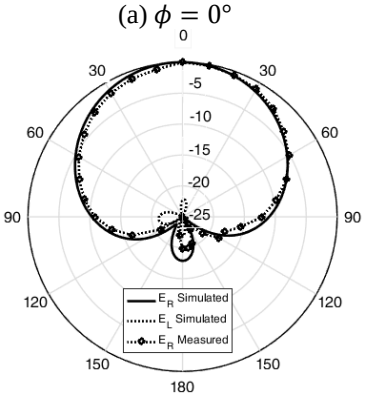

(b) $\phi = 90°$

Fig. 16. Simulated radiation patterns for RHCP and LHCP with the angle θ for two-element array arranged along x-axis compared with the experimental measurements at 4 GHz.

The three-dimensional radiation pattern produced by 20×10 elements array of circularly polarized microstrip patch antenna is presented in Fig. 19 compared to a sketch of the desired three-dimensional beam where the latter is drawn using a dashed line.

As shown in Fig. 20, the radiation efficiency for the final array is about 64% for a lossy FR4 substrate material whereas is about 93% for low-loss FR4 substrate.

It may worthwhile to mention that the antenna array designed in [5], [6], [19] and [20] produces circular polarization for synthetic aperture radar. However, this array produces pencil beam that is steerable over a specific angular range. The present paper is concerned with the design of an antenna array that produces a shaped-beam to get uniform illumination within the beam footprint on the ground surface in both the range and azimuth directions. Nevertheless, we have included discussions of the published results mentioned in Table 1.

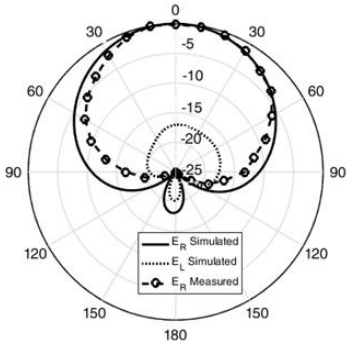

(a) $\phi = 0°$

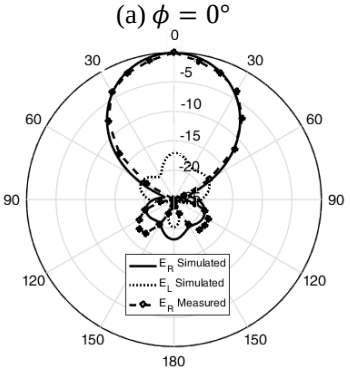

(b) $\phi = 90°$

Fig. 17. Simulated radiation patterns with θ for two-element array arranged along y-axis compared with the experimental measurements at 4 GHz.

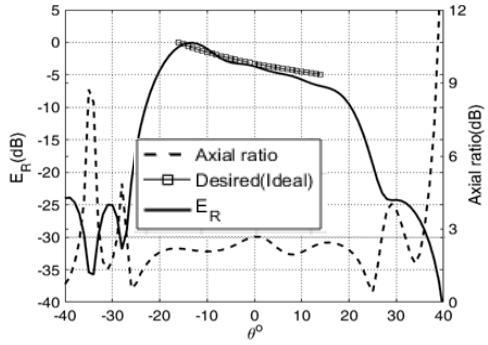

(a) Cosecant-squared beam shape in the plane $\phi = 0°$

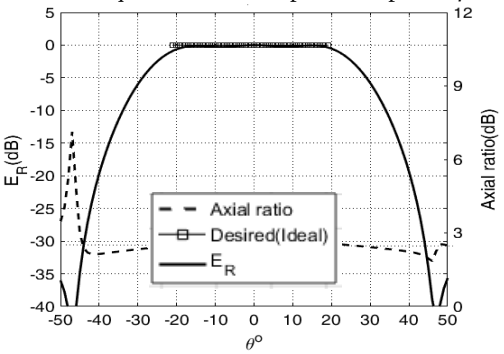

(b) Flat-top beam shape in the plane $\phi = 90°$

Fig. 18. Shaped beam and axial ratio for planar array of 20×10 elements.

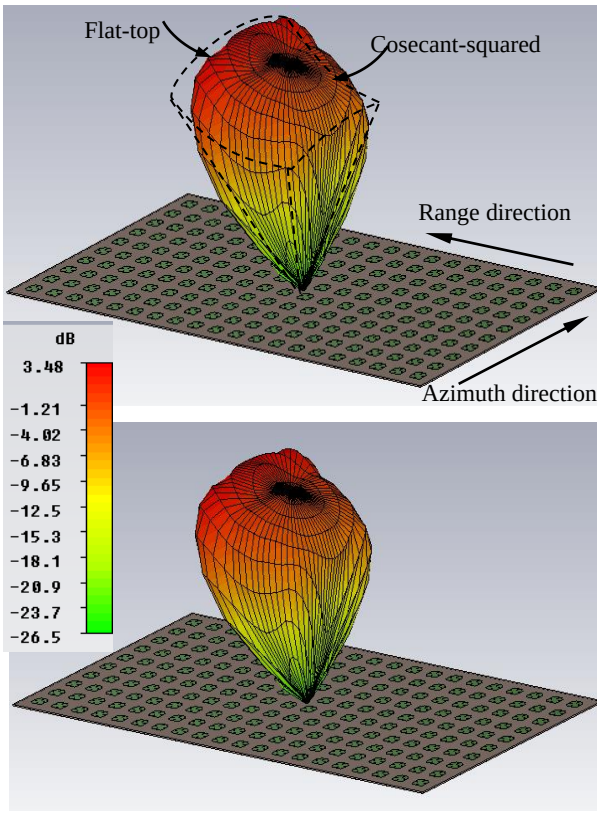

Fig. 19. 3D patterns (cosecant-squared/fan-shaped) synthesized by planar array of 20×10 elements at 4.0 GHz (top figure) and 4.05 GHz (bottom figure).

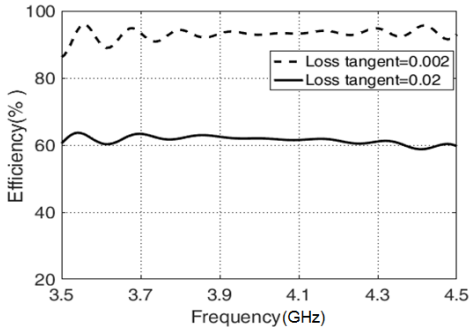

Fig. 20. Antenna efficiency against the frequency.

Table 1: Comparative performance parameters between the present work achievement and that of [19]

Parameters	Reference [19]	Present Work
Frequency	1.27 GHz	4.0 GHz
Axial ratio	≤3 dB	≤3 dB
Efficiency	80%	64%
Azimuth beamwidth	≥ 6.77°	40° (Shaped Beam)
Elevation beamwidth	3.57-31.02°	30° (Shaped Beam)
Antenna size	810×325mm	614×314mm
Polarization	RHCP + LHCP	RHCP + LHCP

VI. CONCLUSIONS

An array of microstrip patches is proposed for SAR systems which can produce either RHCP or LHCP. The effects of mutual coupling between two adjacent elements on the array performance are studied for different separation distances between the elements. The optimum separation between the contiguous elements is determined. Finally, a planar array of 20×10 elements is designed and optimized by applying the PSO algorithm to obtain the beam shape required for land imaging side-looking SAR system, which is cosecant-squared in the range direction and flat-top in the azimuth direction. When compared with the desired beam shapes, the achieved patterns show excellent agreement and the array performance regarding the impedance matching and the axial ratio are acceptable over the operating frequency band.

REFERENCES

[1] Y. Kim and R. Jordan, "Spaceborne SAR antennas for earth science," *Spaceborne Antennas for Planetary Exploration*, pp. 305-340, 2006.

[2] A. K. Behera, A. Ahmad, S. K. Mandal, G. K. Mahanti, and R. Ghatak, "Synthesis of cosecant squared pattern in linear antenna arrays using differential evolution," *In Information and Communication Technologies* (ICT), *IEEE Conference*, pp. 1025-1028, 2013.

[3] A. Freeman, et al., "Detection, estimation and correction of Faraday fotation in linearly polarized SAR backscatter signatures," 1998.

[4] P. Rizki Akbar, J. Tetuko S. S., and H. Kuze, "A novel circularly polarized synthetic aperture radar (CP-SAR) system on board a spaceborne platform," *International Journal of Remote Sensing*, vol. 31, no. 4, pp. 1053-1060, Feb. 2010.

[5] J. Tetuko S. S., V. C. Koo, T. S. Lim, T. Kawai, T. Ebinuma, Y. Izumi, M. Z. Baharuddin, and S. Gao, "Development of circularly polarized synthetic aperture radar on-board UavJX-1," *International Journal of Remote Sensing*, pp. 2745-2756, 2017.

[6] J. Tetuko, S. Sumantyo, and K. V. Chet, "Development of synthetic aperture radar on board unmanned aerial vehicle," *Geoscience and Remote Sensing Symposium (IGARSS, IEEE International)*, pp. 2301-2304, 2013.

[7] M. A. Rahman, Q. D. Hossain, and E. N. I. Toyoda "Design of an X-band microstrip array antenna for circular polarization," *8th International Conference on Electrical and Computer Engineering*, 20-22, Dec. 2014.

[8] K. K. Chan, A. Tan, and K. Rambabu, "Decade bandwidth circularly polarized antenna array," *IEEE Transactions on Antennas and Propagation*, vol. 61, no. 11, Nov. 2013.

[9] X. Ye, M. He, P. Zhou, and H. Sun, "A compact

single-feed circularly polarized microstrip antenna with symmetric and wide-beamwidth radiation pattern," *International Journal of Antennas and Propagation, Hindawi Publishing Corporation*, 2013.

[10] Nasimuddin, Z. N. Chen, and X. Qing, "Asymmetric-circular shaped slotted microstrip antennas for circular polarization and RFID applications," *IEEE Trans. Antennas Propagation*, vol. 58, no. 12, Dec. 2010.

[11] J. James, *Handbook of Microstrip Antennas*. vol. 1, IET, 1989.

[12] A. Qing, *Differential Evolution. Fundamentals and Applications in Electrical Engineering*. John Wiley & Sons (Asia) Pte Ltd., pp. 335-351, 2009.

[13] F. J. Ares Pena, J. A. Rodriguez-Gonzalez, E. Villanueva-Lopez, and S. R. Rengarajan, "Genetic algorithms in the design and optimization of antenna array patterns," *IEEE Trans. Antennas Propag.*, vol. 47, pp. 506-510, Mar. 1999.

[14] J. A. Rodriguez, L. Landesa, J. L. Rodriguez Obelleiro, F. Obelleiro, F. Ares, and A. Garcia-Pino, "Pattern synthesis of array antennas with arbitrary elements by simulated annealing and adaptive array theory," *Microw. Opt. Technol. Lett.*, vol. 20, no. 1, pp. 48-50, Jan. 1999.

[15] L. Xie, Y. Li, and Y. Zheng, "A wide axial-ratio beamwidth circularly polarized microstrip antenna," *IEEE International Conference*, 2016.

[16] J. Robinson and Y. R. Sammi, "Particle swarm optimization in electromagnetics," *IEEE Transactions on Antennas and Propagation*, vol. 52, no. 2, pp. 397-407, Feb. 2004.

[17] M. Abo El-Hassan, K. F. A. Hussein, A. E. Farahat, and K. H. Awadalla, "Wide band shaped beam array of U-slot patches for high resolution SAR and satellite communications," *34th National Radio Science Conference (NRSC 2017), Arab Academy for Science, Technology & Maritime Transport, (Abou Qir)*, Alexandria, Egypt, B14, Mar. 13-16, 2017.

[18] W. L. Stutzman and G. A. Thiele, *Antenna Theory and Design*. 3rd Edition, Wiley, New York, pp. 319, 2012.

[19] V. Wissan, "Development of circularly polarized array antenna for synthetic aperture radar sensor installed on UAV," *Progress in Electromagnetics Research*, 19, pp. 119-133, 2011.

[20] M. Baharuddin, "Study on circularly polarized synthetic aperture radar: Patch array antennas and scattering experiments in an anechoic chamber," *Ph.D. Thesis*, Chiba University, 2016.